Clay Characterization of Tiller Flotten Quick Clay

René Tammen[a], Kamila Zabłocka[b], Klaartje De Weerdt[b], Erika Eiser[a,c]

[a] *Porelab, Dept. Physics, Norwegian University of Science and Technology, Høgskoleringen 5, Trondheim, NO-7491, Trøndelag, Norway*
[b] *Department of Structural Engineering, Richard Birkelands vei 1A, Trondheim, NO-7491, Trøndelag, Norway*
[c] *Cavendish Laboratory, University of Cambridge, JJ Thomson Avenue, Cambridge, CB3 0HE, Cambridgeshire, United Kingdom*

Abstract

In this study, we investigate the mineralogical and physicochemical properties of the Tiller–Flotten quick clay formation in Trondheim, Norway. The objective is to enhance our understanding of particle interactions within this quick clay system, thereby contributing to the development of more environmentally friendly stabilization strategies. A comprehensive suite of analytical techniques was employed, including X-ray diffraction (XRD), X-ray fluorescence (XRF), and energy-dispersive spectroscopy coupled with scanning electron microscopy (EDS-SEM). Compared to other quick clay formations, biotite was found to be the most abundant clay mineral, followed by illite and chlorite. The specific surface area (SSA) was determined to be $\sim 28\,\mathrm{m^2 g^{-1}}$, and the cation exchange capacity (CEC) was less than $4\,\mathrm{meq100g^{-1}}$. These findings may help explain the distinct behavior of the Tiller–Flotten quick clay compared to other formations. Zeta-potential measurements were conducted using different salts at concentrations of $25, 50$, and $100\,\mathrm{mmol/L}$. Among those, $MgCl_2$ and $CaCl_2$ induced the most significant changes in the zeta potential. The other salts (NaCl, KCl, K_2SO_4, K_2CO_3, and KOH) resulted in more negative zeta potentials of $-50\,\mathrm{mV}$ compared to the initial value of $-32\,\mathrm{mV}$ in distilled water. Increasing the concentration of those salts led to a reduction in the diffuse double layer. However, even at $100\,\mathrm{mmol/L}$, the zeta potential changed only slightly. Additionally, K_2CO_3 and KOH significantly increased the pH to 10-12, further influencing the electrochemical behavior of the clay particles.

Keywords: Tiller Flotten, quick clay, illite, biotite, elemental analysis, crystal structure

1. Introduction

Quick clay is a sensitive metastable clay formation characterized by a remolded shear strength of less than 0.5 kPa (1). When disturbed, those formations show catastrophic fluidization turning into potentially deadly landslides. The slide itself is characterize by rapid and retrogressive movements (2). A famous example is the quick-clay event in Rissa, Norway in 1978. An estimated 5-6 km^3 of clay-rich land slid into the ocean, destroying several houses, costing the life of one person and causing a 3 m high tsunami. A more recent case is the event in Gjerdum, close to Oslo, which occurred in 2020. This landslide cost ten lives (3). The greatest quick-clay event in Norway occurred in Verdal, in 1893. More than 3 km^3 of cultivated land disappeared and killed more than 111 people (4). Other cases of quick-clay induced landslides occur regularly in Sweden, Finland, Russia, Canada, and the USA (5; 6; 7). To prevent such catastrophic events from happening, large efforts are undertaken to detect quick clay in the ground and subsequently stabilize it with lime cement. Although stabilization of quick clay with lime cement is cost effective, this procedure contributes to the $\sim 8\,\%$ of CO_2 emission produced worldwide. About 1 ton of CO_2 per 1 ton of lime cement is created (8): $CaCO_3$ + heat $\rightarrow$ CaO + CO_2.

To reduce the CO_2 emission in lime-cement production, different types of binders such as fly ashes (9), biochar(10) or other waste products (11; 12) are being used. Because a detailed structural and compositional analysis of quick clay presents a geotechnical challenge, soil analysis often stops at the macro-scale. To develop a new, sustainable ground stabilizer and reduce global CO_2 emissions, it is crucial to fully understand the quick-clay system. This includes gaining a deeper understanding of illite, which is considered the primary component that influences the structure of quick clay.

One problematic aspect is that the term 'illite' is often used as a generic name. Early 2025, Helle and Aagaard (13) reported that illite clay in Norway is created through geo-mechanical (detrital) rather than weathering (authigenic) processes. Therefore, the present Norwegian illite is a mixture of fine-grained muscovite and biotite rather than true illite.

Although several studies report XRD results, which indicate that illite is the dominant clay mineral in quick clay, one needs to be cautious using this interpretation. The XRD patterns of illite, muscovite, and other 2:1 phyllosil-

icates all exhibit a strong Bragg peak at around 10 Å, making them difficult to distinguish them from one another. Moreover, the complexity of natural materials often leads to overlapping peaks and ambiguous identifications in XRD analyses.

Given the goal of developing alternative stabilization strategies for quick clay, based on its physical and chemical properties rather than simply its clay content, it becomes essential to accurately determine the true nature of the clay minerals present.

In this study, we investigate the unique properties of quick clay from Tiller Flotten, located near Trondheim, Norway. Using a comprehensive suite of analytical techniques, we characterize the mineralogical composition and crystal structures of the clay with X-ray diffraction (XRD), X-ray fluorescence (XRF), and energy-dispersive spectroscopy coupled with scanning electron microscopy (EDS-SEM). To explore the electrochemical behavior of the clay particles, we combined the calculated surface charge data with zeta potential measurements and examined the influence of seven different salt solutions. Furthermore, we determined the specific surface area (SSA), pore size distribution, and cation-exchange capacity (CEC) using the BET (Brunauer, Emmett, Teller), the BJH (Barrett, Joyner, Halenda), and the methylene-blue spot test. Together, these experimental results provide a deeper understanding of the mechanism of how quick clay is formed and the complex interparticle-interactions that govern its behavior.

2. Background

2.1. Quick clay concept

To understand the mechanisms behind a quick-clay landslide event, it is essential to first examine the geological origin and environment in which such deposits can form.

Norwegian geomorphology was shaped mainly by repeated glacial periods. Quick-clay deposits formed during the Younger Dryas period (12900 to 11700 years ago) (14), which experienced an abrupt return to near-glacial conditions. During this time, a continental ice sheet of up to ~ 2000 m (15) covered the bedrock, causing an isostatic depression (16). As the ice began to melt in the mid Younger-Dryas period, the depressed land surface remained below sea level, allowing marine waters to flood the region. For instance, the area around Trondheim was submerged about 175 m (17).

The material that sedimented stemmed mainly from glacial erosion of greenstone, meta-sediments and volcanic debris. The reported mineralogy of the resulting quick clay often consists of quartz, feldspar, and clay minerals (7). In some regions, hornblende and other minerals were also found. However, the main clay minerals mentioned in literature are illite and chlorite. Although, other clays such as smectite and muscovite were also reported (18). Because both illite and muscovite display very similar XRD peaks, it is difficult to distinguish these two closely related phyllosilicates.

Due to chemical substitutions such as the replacement of Si^{4+} by Al^{3+} in the tetrahedral layers or Al^{3+} by Mg^{2+} or Fe^{3+} in the octahedral sheet, clay particles carry a natural negative surface charge, which causes the formation of a diffuse double layer (DDL) in aqueous solutions (see Figure 1). The thickness of this layer, referred to as the Debye screening length (λ_D), quantifies the distance over which electrostatic interactions are screened in solution. It is defined as

$$\lambda_D = \sqrt{\frac{\varepsilon_0 \varepsilon_r k_B T}{n_e q^2}},$$

where ε_0 is the vacuum permittivity, ε_r the relative permittivity, k_B the Boltzmann constant, T the temperature, n_e the electron number-density and q the charge of the ions in solution (19).

For instance, in distilled water the DDL of charged particles is relatively thick. Under these conditions, the repulsive Coulomb interactions between equally charged particles stabilize their dispersion. However, in a highly saline marine environment, Na^+ ions screen the negative surface-charges of the flat clay-particle surfaces. In other words, the Coulomb repulsion becomes sufficiently short-ranged for the attractive van der Waals interaction between the particles to dominate, which leads to flocculation.

Rosenqvist (2) suggested that quick clay forms when clay minerals (present in glacial melt water) are suddenly exposed to highly saline water. Under such conditions, the finest clay fractions flocculate rapidly, thus forming large clusters that subsequently sediment at rates similar to those of coarser particles. These fast sedimentation speeds lead to loosely packed, open frameworks commonly referred to as 'house-of-cards' structure (20).

As the weight of the glacial ice diminished, the landmass began to rise, a process known as isostatic rebound, which continues to this day. This uplift gradually brought the marine clay deposits above sea level. Once exposed to freshwater infiltration, for example through rain, these clay deposits started

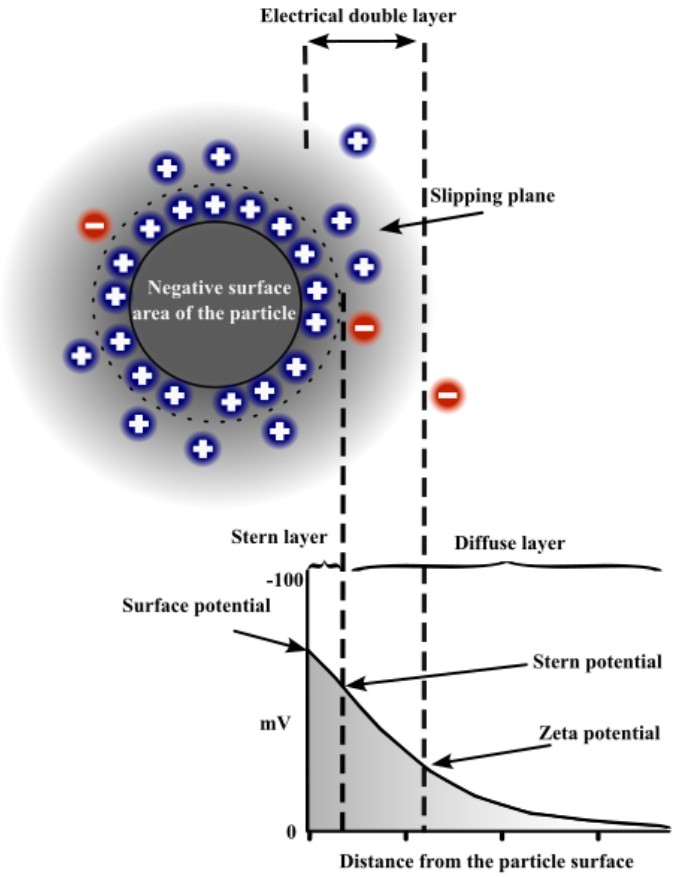

Figure 1: Illustration of the diffuse double layer and Debye screening length around a negatively charged, spherical particle suspended in water.

to leach out the salt that was present in the marine environment. This process reduced the ionic strength of the pore water, leading to a thickening of the diffuse double layer. The increased electrostatic repulsion between particles weakens the interparticle attraction, making the clay structure metastable and more susceptible to collapse under shear stress.

2.2. Clay particle and clay minerals

Clays are ubiquitous and play an important role in our daily life, ranging from agriculture to paper production and flow modifier in cosmetic and other industries (21). However, the term 'clay' does not have a unique definition. In 1546, Georgius Agricola formulated the first definition of clay (22). Since

then, this definition was revised numerous times. Nevertheless, it still contains the main original factors: clays are fine-grained, naturally occurring materials, which are plastic when wet but harden when dried or fired (23).

Interestingly, even though all disciplines have introduced an upper limit of the particle size below which all soils are called clays (ranging from 1 μm to 4 μm) there is no official upper particle size. Geologists and other researchers also distinguish between the term clay and clay mineral, with latter having an equally broad definition. Clay minerals are often phyllosilicates but also minerals, which show plasticity and hardening upon drying/firing on macroscopic scale. Moreover, clay minerals are not defined by their crystal size (22). In his book "Illite", Meunier argued that size should not be a criterion for a mineral group (24). He pointed out that some definitions for illite consider size as criterion for it to be a mineral. Therefore, everything above 4 μm is a mica and not an illite, regardless of their crystal structure.

2.3. Illite

In 1937, Grim introduced the term illite, naming it after the US-state Illinois, to describe a mica-like clay mineral group (25). Since Grim's first publication on illite, demonstrating the difference to the well know clay mineral mica, the characterization of Illite has been extended.

Illite is generally classified as a 2:1 phyllosilicate, consisting of one aluminum octahedral sheet sandwiched between two silicate tetrahedral sheets (see Figure 2). Potassium ions (K^+) are fixed within the hexagonal cavities of the tetrahedral sheets, forming strong interlayer bonds that prevent significant ion exchange between layers (26). As a result, illite is considered a non-expandable clay mineral with a consistent basal spacing of approximately 10 Å (24; 27). The degree of isomorphic substitution in illite is lower than in muscovite. While muscovite typically exhibits around 25 % substitution, illite shows approximately 16 % (27; 28). Additionally, illite contains less potassium and more interlayer water than muscovite, further distinguishing its structural and chemical properties.

However, 60 years after the initial definition of illite, Rieder et al. (1998) (29) noted it still lacks a precise mineralogical definition and is best regarded as a mineral series, often considered a counterpart to glauconite. One of the major challenges in defining illite is its structural variability: it exists in multiple polytypes and rarely occurs in pure form in nature. This complexity makes its classification and characterization difficult, especially when distinguishing it from closely related mica-group minerals.

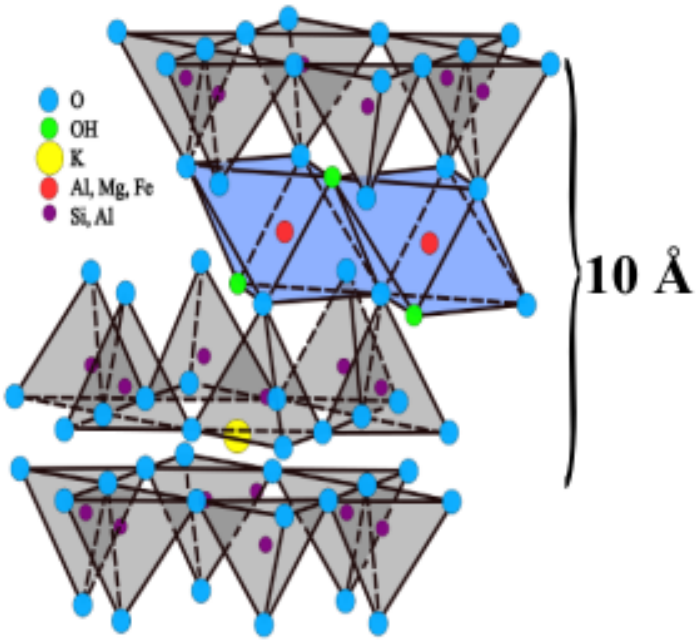

Figure 2: Crystal structure of illite after Grim 1982.

3. Material

The material was sourced from the Tiller Flotten area in Trondheim, Norway, from depths between 7 and 17 m. We name the samples TF7 and TF17, respectively. When referring to TF only, measurements in either depth were performed, as we did not observe many changes. The expected clay content at both depths is estimated to vary between 20 and 60 % (7). In addition, we used purified illite, purchased from MuseChem, USA. The data sheet of this material lists a composition of 94.2 % illite, 2.1 % anatase, 3.5 % diaspore, and 0.2 % rutile. In the following, we will present our own analysis, which shows that the commercial sample is not illite but a mixture of two types of muscovites. Nevertheless, as CMS illite was commercially not available, we decided to use this material as a proxy. Here, we will refer to the commercial proxy as "pure illite". A second reference material we used was Laponite® XLG, which was purchased from Rock Additives. We refer to it as Laponite in the text.

4. Method and Technique

4.1. XRD

For the X-ray diffraction (XRD) measurements, a Bruker D8 Advance Series 2 instrument with a Co X-ray source, was used. Before analysis, the sample was dried and crushed to a particle size of approximately 10 μm. XRD analysis is based on Bragg's Law

$$n\lambda = 2d\sin(\theta)\,,$$

where $\lambda = 1.789\,\text{Å}$ is the wavelength of the Co source, d is the lattice spacing for a given set of Miller indices and n is the order of the Bragg peaks observed under the scattering angle θ. Thermal effects on mineral phases were investigated by conducting XRD measurements after heating the sample to 300, 550, 750, 950 and 1100 °C. For each temperature, the sample was placed in an oven and kept for 2 hours before the measurement.

To assess the swelling capacity of the clay, the material was treated with ethylene glycol. For this analysis, the sample was further ground to a finer particle size of $\sim 6\,\mu m$. We used the Diffract.EVA6 and TOPAS 5 instruments for mineral identification, refinement and quantitative analysis and the Open Crystallographic Database were used to analyze the data.

4.2. XRF

The x-ray Fluorescence spectrometer from Malvern Panalytical Zetium XRF instrument (operated with a 4 kW X-ray source) was used to measure the representative oxides in the bulk quick clay material. The instrument was calibrated using the WROXI Certified Reference Material. Moreover, this method allowed us to measure the Loss of Ignition (LOI).

4.3. SEM and EDS

We performed scanning electron microscopy (SEM) measurements using a Hitachi-S2300N instrument, which was equipped with a thermionic electron emission gun, a SE, BSE and an energy-dispersive X-ray spectroscopy (EDS) detector. Latter was used to determine the elemental composition of the materials analyzed.

4.4. TGA and DTG

Thermogravimetric analysis (TGA) and derivative thermogravimetry (DTG) were performed using a Mettler Toledo TGA instrument operated under a nitrogen atmosphere. The experiments were conducted in a temperature range of 40 to 1100 °C at a heating rate of 10 °C min^{-1}. TGA measures the change in sample mass as a function of temperature, while DTG records the rate of mass loss. These techniques enable the identification of mass-loss events during heating, such as the removal of adsorbed water, dehydroxylation of clay minerals, and the release of CO_2 from carbonate decomposition.

4.5. SSA, Pore size, and CEC

The specific surface area (SSA) and pore sizes were determined with a Micromeritics, Tristar II Plus instrument, which allowed us to conduct BET and BJH measurements. For this, the clay was dried and sieved using a mesh-size $< 63\,\mu$m. Subsequently, the samples were dried at 90 °C. To remove water completely the samples were degassed using the Micromeritics oven over night. The SSA value was assessed further using the methylene blue spot test, which allowed us to estimate the cation exchange capacity (CEC) of the sample.

4.6. Particle size distribution

We used two methods to determine the typical particle sizes.

4.6.1. Laser Diffraction using the Mastersizer 3000E

In this method, the sample material was dried at 90 °C before measurement. Less than 1 gram of the dried material was then transferred to a beaker to which we added 1 mL deionized water. The suspension was then sonicated to disperse the particles. The instrument's software monitors the suspension to ensure stability and no further change in particle sizes before initiating the measurement. The average particle size and size distribution are measured using light scattering.

4.6.2. Hydrometer Analysis

This method, commonly used in soil science for fine particles, is based on the Stokes-Einstein equation: $D = k_B T/(6\pi\eta R)$. Here, k_B is the Boltzmann constant, T the temperature, η the dynamic viscosity, and R the particle radius.

Two 1 L cylinders were prepared using distilled water and 20 g of sodium pyrophosphate ($Na_4P_2O_7$*$10H_2O$). One cylinder served as a reference (zero reading for the hydrometer). The quick clay was sieved through a 75 μm mesh and washed with approximately 200 mL of the prepared solution. The material retained on the sieve was dried overnight to analyze the coarse fraction. The washed clay collected in the first bowl was transferred to a second bowl. The first bowl was rinsed with additional solution to minimize material loss, and the contents of both bowls were combined and poured into the test cylinder. The cylinder was sealed with a stopper and shaken for 1 minute to resuspend the particles. Immediately after removing the stopper, the hydrometer was inserted, and readings were taken at 0, 1, and 2 minutes. Between measurements, the hydrometer was returned to the reference cylinder. The test cylinder was then shaken again, and further readings were taken at 5, 10, 20, 40, 80, 160, and 320 minutes, with the final measurement taken after 22 hours. After the final reading, the suspension was transferred to a bowl and oven-dried to determine the dry mass and calculate the initial water content of the sample.

4.7. Zeta Potential

Zeta potential measurements were conducted using a Malvern Panalytical NanoSizer. A quick-clay suspension with a concentration of 133 gL^{-1} was prepared. The clay was dispersed in seven different salt solutions: NaCl, $MgCl_2$, KCl, $CaCl_2$, KOH, K_2CO_3, and K_2SO_4. Each salt was tested at three concentrations: $25, 50$, and $100\,mmolL^{-1}$. For each condition, three independent suspensions were prepared and each was measured in triplicate to ensure reproducibility. The pH of all solutions were measured using a calibrated pH meter.

5. Results

Quick clay from Tiller has been studied since the 1980s. It contains the typical minerals for Norwgian quick clay, such as quartz, feldspar and clay minerals (7). However, the exact clay-mineral elemental composition is often neglected, which is essential to understand and develop new stabilization methods. In the following we present a systematic study that reveals that what we know as illite is in fact a mixture of other mica-like minerals.

5.1. Water Content

Quick clays typically contain a high amount of water, often exceeding 40 %, due to their characteristic "house-of-cards" structure (2; 7; 30; 31). To estimate the water content, several unpurified samples were oven-dried at 90 °C until no significant weight loss was observed. The measured weight loss ranged from 35 to 50 wt%. The dried samples were subsequently used for XRD and EDS-SEM analyses.

5.2. Fraction Separation

To separate the clay-sized particles from the bulk we followed the gentle purification process described by Bergaya et al. (32) with small deviations. In brief, $\sim$ 35 g of fresh quick clay was diluted in 200 ml of a 1 M NaCl solution (prepared by mixing 200 ml of distilled water with 11.7 g NaCl) in a beaker. The beaker was placed on a magnetic stirrer overnight, stirring at 200 rpm for at least 12 hours. After 12 hours, the mixture was divided into six 50 ml tubes for centrifugation. Each tube was filled up to the 40 ml mark. The centrifuge was operated at 3000 rpm for 2 hours. During centrifugation, clay-sized particles settled at the top, while heavier materials moved to the bottom of the sediment. When a clear layer between the top and bottom was visible, the top layer was gently removed for further processing. This procedure was repeated six times with the remaining material to ensure thorough interaction between clay particles and salt, facilitating separation from the rest of the material.

After six repetitions, the centrifugation settings were adjusted to 7000 rpm for 3 hours, creating a clear layer, with the first layer representing our clay sample. The clay was then re-dispersed in deionized (DI) water and centrifuged three times to separate any residual materials. After this step the solutions were placed in a dialysis bag in a bowl of distilled water for seven days, to remove the salt. The distilled water was changed daily. Note that we avoided using chemicals that may influence the structure or dissolve the clay particles.

The clay suspension was then dried in an oven at 90 °C over night, and subsequently freeze-dried for 2-4 days. Since this process is time consuming it has been only used for EDS measurements, where we compared the dried samples containing all fractions with the top sediment that is rich in clay minerals (see greenish layer in Fig. 3).

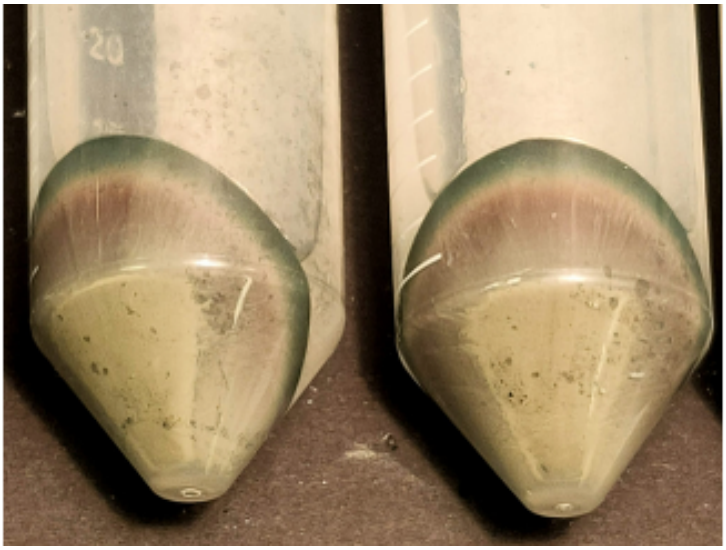

Figure 3: Layered material from Tiller Flotten quick clay, TF7, after the last centrifugation of the purification process. The greenish top layer contains clay-sized particles and thus a higher percentage of the clay minerals, which we used for EDS measurements; the bottom material holds silt and sand-sized particles.

5.3. XRD-Spectra and Interpretation

First we employed XRD measurements at 25 °C to determine the mineralogy content in the samples. In Figure 4 we show the XRD pattern of a Tiller Flotten quick clay, TF7, and that of the pure illite reference sample. The inset shows the difference between the glycol-treated (red) and untreated (black) XRD patterns, which will be discussed in greater detail later.

The pure illite (Figure 4A) displays a relatively smooth XRD-profile with fewer peaks than the TF7 sample (Figure 4B). When using the match-finding function of DIFFRACT.EVA with no chemical filters, the software suggests the presence of muscovite with 59.7 % and illite with 37.2 %. This highlights the challenge of distinguishing illite from muscovite via XRD without additional information. The remaining percentage splits into rutile, anatase and diopside. However, when applying Rietveld refinement to our data in TOPAS, we rather find two different types of muscovite and no or low amounts of illite. Still, we use the so-called pure illite as a reference to the TF samples, since there was no other illite standard available on the market during our work. Our analysis provides the following distribution of the minerals in the reference illite: muscovite 66.17 %, illite 27.73 %, diaspore

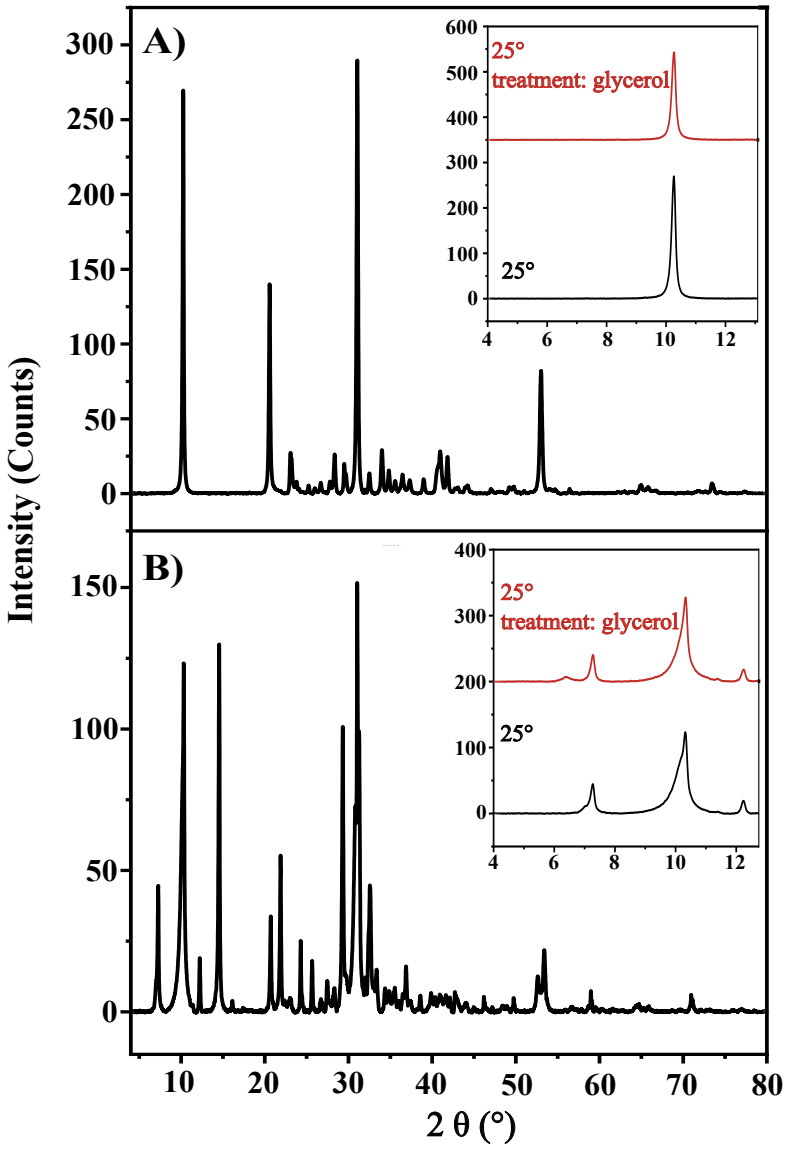

Figure 4: XRD patterns obtained for (A) pure illite and (B) Tiller Flotten quick clay from a depth of 7 m. The insets compare the XRD patterns before and after glycol treatment at around $2\theta = 10\,^{\circ}$. All measurements were performed at 25 °C.

3.26 %, anatase 1.61 %, and rutile 1.03 %.

Already Zhuo and coworkers (33) stated that the quantification of clay minerals is a complex undertaking, because clay minerals have unique structures with various polytypes that can vary in chemical composition. Hence, even though simple XRD measurements represent a powerful tool, it might not be enough to clarify, which clay mineral is present without any additional information.

The natural TF7 exhibits more peaks than our pure illite sample because of the lager variation in minerals. Several mineral phases are clearly identifiable: We detected quartz (18.2 %), K-feldspar (2.7 %), plagioclase in the form of albite (9.4 %) and hornblende (5.3 %), along with additional minor phases such as microcline and calcite (total: 0.88 %). Those findings compare well to previous research (34; 35).

In terms of clay minerals, chlorite (14.2 %) was identified together with a small amount of kaolinite (4 %). Both clay minerals exhibit similar peak positions. To distinguish between chlorite and kaolinite, the sample was heated to 550 °C. At this temperature, kaolinite loses its structure and becomes amorphous, which is reflected in the decrease in scattering intensity around $2\theta = 12°$. If chlorite is present, the peak at $2\theta = 10°$ increases significantly. Both effects are observed in Figure 5.

The scattering intensities around 10° amount to biotite (21.5 %), muscovite (15.2 %), and illite (12.8 %). An additional low percentage of swelling clays such as smectite and vermiculite could be detected.

Biotite in quick clay can be found in many research studies. However, normally it appears only in small amounts in the bulk material and is hardly present in the clay-particle sized fraction (18). The reason for that is the fast weathering of biotite, which converts to vermiculite or chlorite (36). The presence of biotite we find in the clay-fraction size can be explained by the geological history, in which the clay was ground into finer sizes by the ice sheet. One might also argue that we conducted the measurements with the entire dried TF samples that were ground to roughly 10 μm. However, in 2022, Hov et al. (37) measured TF soil from the same area, but only the clay-sized fraction. Similar to our results they obtained 26 % biotite, while the illite/muscovite fraction was 23 %. We conclude that the dominant clay in the Tiller Flotten region is biotite and not illite, when only XRD measurements are considered.

Although quick clay is often reported to have no swelling potential our tests show slight swelling. This finding aligns with the work by Khaldoun

et al. (38). Latter also claimed that the quick clay can be only stabilized by adding salt when swelling clays are present.

That quick clay deposits can vary a lot even within a short distance, as is shown by the formation in Dragvoll, which is a few kilometer north of the Tiller Flotten area. For the Dragvoll formation researchers (6) reported from a sample at $\sim 2\,\mathrm{m}$ depth, which was dominated by an amount of $32 - 36\,\%$ chlorite and muscovite each. Only $2 - 5\,\%$ was biotite, while illite was not present, although it is normally believed to be the dominant clay mineral. Yet others reported the presence of illite instead of muscovite (39; 5).

5.3.1. Swelling Potential

Measuring the swelling potential is a key factor in characterizing clay minerals and soil behavior. Mica-like clays such as illite, muscovite, and biotite are classified as non-swelling clays. However, pure illite is rarely found in nature. It exists in various polytypes and often contains smectic interlayers capable of swelling. These mixed-layer structures are referred to as illite-smectite (I/S). In contrast, muscovite and biotite do not possess such interlayers.

To estimate the swelling potential and the I/S ratio, the sample can be treated with glycol. This treatment causes smectic layers to expand, which can be detected by comparing the full width at half maximum (FWHM) of the (001) and (003) planes of illite before and after glycolation, which we measure in XRD. The swelling strength is determined by the intensity ratio

$$I_r = \frac{[(001)/(003)]_{\text{air-dried}}}{[(001)/(003)]_{\text{glycol}}} \ .$$

An I_r value around 1.0 indicates no swelling behavior, while I_r larger than unity reflects the systems' swelling capacity. For the pure illite sample (Figure 4 B)), the calculated I_r value is 0.96, which confirms its non-swelling nature. In contrast, the TF7 sample exhibits a value of 1.42, clearly indicating swelling (red curves in the inset of Figure 4 A). Although it was challenging to determine the FWHM of the (003) peak due to the closeness of adjacent peaks, it provides strong evidence for the presence of smectic layers within the sample. Although, it is not possible to tell whether the smectic layers appear within the illite particles or are present as a separate fraction. We also note that the XRD pattern of the glycole-treated sample shows an additional peak at $2\theta \sim 6\,^\circ$ while the peak at $2\theta \sim 10\,^\circ$ is getting slimmer and smoother.

In literature it is often stated that quick clay is non-swelling (40; 41). However, Rosenqvist (42) reports that clay minerals that constitute quick clay undergo a weathering process in shallow layers that do not exceed 4 m. These superficial layers are exposed to atmospheric conditions, often undergoing drying/re-hydrating cycles. This weathering process can lead to the conversion of illite to a montmorillonitic mineral, which is well known for its swelling potential. Even though our sample is from a depth of 7 m, we believe that the large temperature cycles in Norway may extend this weathering process to greater depths.

5.3.2. Heat treatment

Another method to confirm the presence of different 2:1 phyllosilicates in the Tiller Flotten clay is to measure the dehydroxylation (DHX) temperatures, which tend to differ from one clay mineral to another. Typically illite is less heat resistant than muscovite and biotite. In general, the DHX temperature (endothermic reaction) for illite starts at $\sim 525\,^{\circ}\mathrm{C}$ (43), undergoing the following reaction:

$$\mathrm{KAl_2(Si_3Al)O_{10}(OH)_2 + H_2O \rightleftharpoons KAl_2(Si_3Al)O_{11}}$$

Muscovite, on the other hand, has DHX temperatures that vary between 800 and 900 °C, while biotite shows a change only over 1000 °C. However, at 400-500 °C and 800 °C structural alterations appear (44).

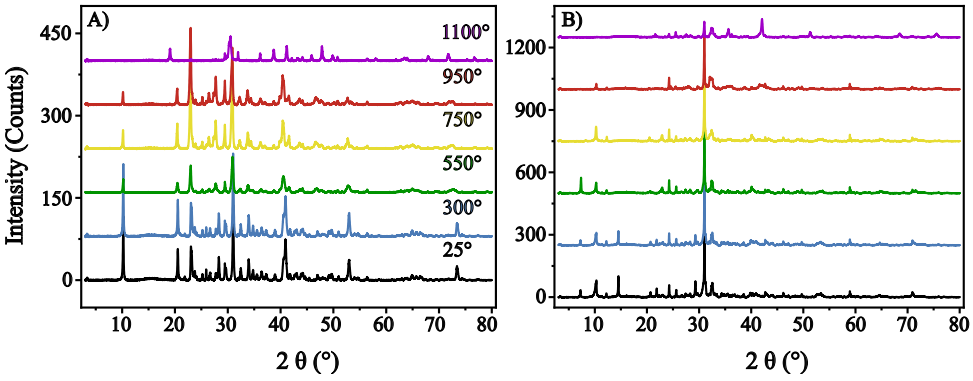

Figure 5: XRD patterns of (A) pure illite and (B) Tiller–Flotten quick clay (7 m depth) after heating to 25 °C (black), 300 °C (blue), 550 °C (green), 750 °C (yellow), 950 °C (red), and 1100 °C (purple).

XRD measurements in the pure illite sample (Figure 6 A) show that the intensities of the first two peaks start to decrease at 550 °C due to DHX. However, at around 750 °C their intensities increase again to then diminish at 950 °C. Finally, at 1100 °C the XRD intensities change entirely. The main peaks at $2\theta = 10\,^{\circ}$, $32\,^{\circ}$ and $42\,^{\circ}$ vanish, and a new peak starts to appear at $2\theta \approx 19\,^{\circ}$, which indicates a phase transition to the clay mineral mullite (43).

In the quick-clay sample TF7m (Figure 6 B) the XRD pattern shows a double peak at around $2\theta = 10\,^{\circ}$. It reduces to a single peak at 550 °C. Also note that the peaks at $2\theta \approx 7.2\,^{\circ}$ and $14\,^{\circ}$, show the presence of chlorite. The intensity of the first chlorite peak increases strongly until about 550 °C to then disappear at higher temperatures. Conversely, the second chlorite peak decreases continuously and vanishes above 550 °C. The additional peaks in the XRD pattern, which originate from other minerals present (e.g. hornblende, feldspar and quartz) seem less affected by the heat treatment, as they show a phase transition due to DHX only above 950 °C. Comparing the pure illite structure with that of the TF7m sample, latter did not show a transition to mullite at 1100 °C. Instead, we found magnetite, which typically forms at these high temperatures. The magnetite formation, enhanced by the relatively high Fe content of the quick clay sample (see XRF and EDX measurements) may also be responsible for the suppression of the transition to mullite.

5.4. TGA and DTG

To gain deeper understanding of the heating reaction of the TF quick clay and the reference material, we also conducted a thermogravimetric (TGA) and differential thermal analysis (DTG).

5.4.1. TGA

TGA measurements provide us with the mass loss of the sample through dehydration and dehydroxylation during heating; the data are presented in Figure 6. Pure illite shows a continuously decaying TGA curve (black) that can be split in three sections. Below 200 °C, we register a weight lost of $\sim 0.6\,\%$, which can be ascribed to dehydration (DHD) of loose water in the clay. In the second section, ranging from 250 °C to 800 °C, the sample loses additional $\sim 5\,\%$ of its initial weight due to DHX processes in the clay structure. The third section, starting above 800 °C, shows only a minimal additional weight lost of $\sim 0.1\,\%$. Hence, the sample loses in total 5.7 % of its starting weight.

The TF7 sample displays a more complex behavior with an initial weight loss of $\sim 1\,\%$ below 200 °C. The region where DHX processes occur can be divided into three parts: (i) for temperatures between 200 and 575 °C the weight lost is $\sim 2\,\%$; (ii) between 575 and 740 °C we observe a weight lost of further 2 %, which is marked by a different slope in the TGA-curve; (iii) this section runs until 1100 °C with a weight lost of 1 %. Here, the total weight lost is $\sim 6\,\%$.

The low weight lost below 200 °C in our TF7 is a good indicator that only a negligible amount of smectic material is present, as expected. Further, the multiple DHX states in our TF7 sample reflects the presence of a mixture of different clay minerals.

5.4.2. DTG

The DTG is the first derivative of mass change with respect to time. It provides information about how fast the mass loss in the sample is during the experiment. This allows the different mass-loss events during heating to be identified more clearly than from the TGA curve alone.

Beginning with the pure illite sample we observe a first mass loss at 200 °C. This peak represents the DHD of the material. Further, mass losses are between 500 and 650 °C. Both peaks are in the typical DHX temperature of illite, as mentioned earlier. A weak DTG peak is observed at approximately 920 °C. This peak may represent the final stage of dehydroxylation of well-crystallized mica. Although spinel-type phases are known to form in this temperature range (45), their crystallization is generally not associated with a measurable mass loss. Therefore, the DTG signal is more likely related to the final release of structural hydroxyl groups. At this stage, the illite structure is largely collapsed and subsequent recrystallization into high-temperature phases, such as mullite, may begin. These results are partly in agreement with our XRD results. However, the reactions appear at lower temperatures in the DTG measurements. These differences may be explained by the different heating rates (46).

The TF7 sample is showing a much stronger mass loss at the DHD than the reference material. This indicates a higher content of physically adsorbed water in the quick clay than in the reference illite. Between 200 and 400 °C, some mass loss can be noticed. This shows the presence of organic material (see SEM images in Fig. 7 and Fig. 8). Additional mass loss peaks are found at 575 °C and 720 °C. The first peak is representing again the typical DHX temperature of illite, while the second peak is a bit above the expected tem-

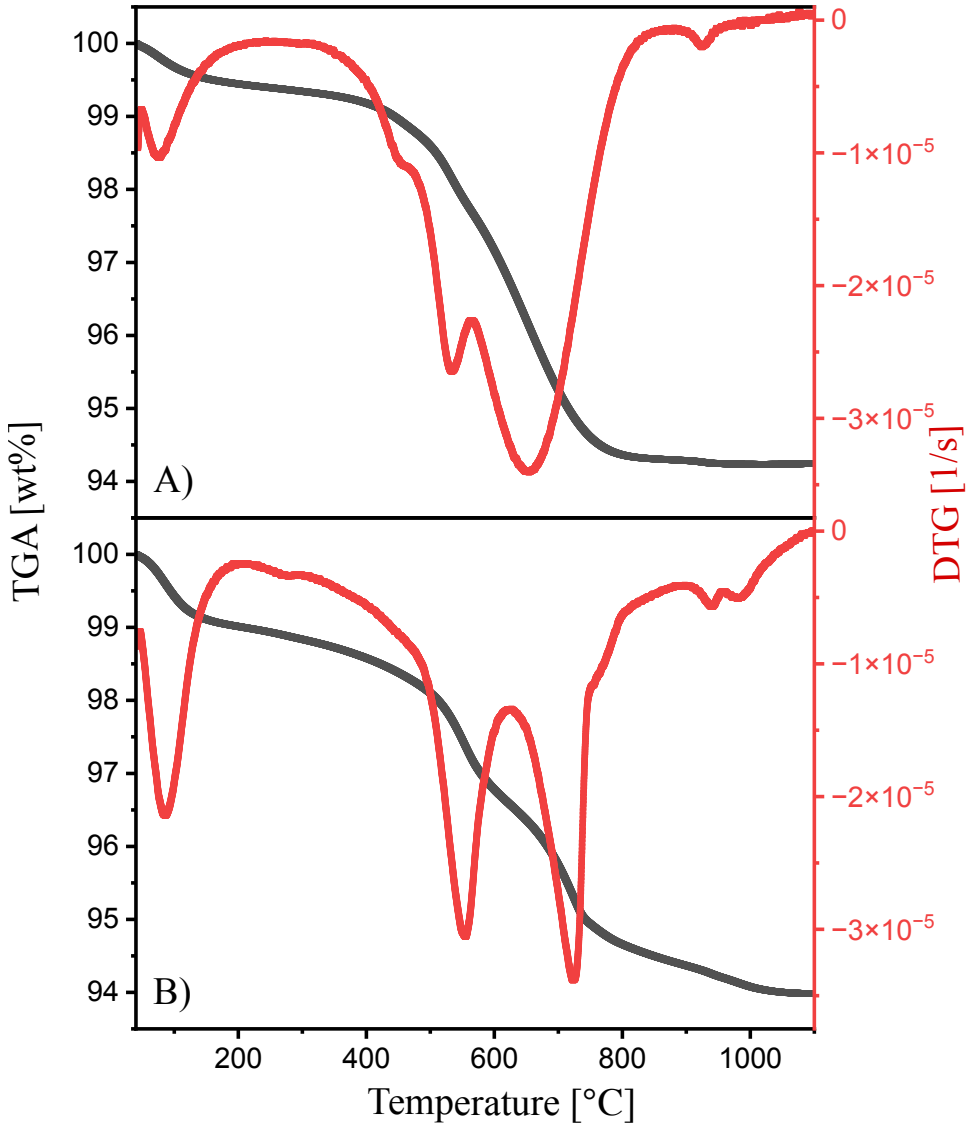

Figure 6: TGA (black) and DTG (red) curves of A) pure illite and B) TF7 sample.

perature range. Also, the typical DHX main peak for muscovite and biotite are at higher temperatures. Such shifts have been observed in disordered

structures preciously (46). Based on the geological history, disordered structures are very likely. Furthermore, interactions between different mineral phases may modify the thermal behaviour of the individual components.

Moreover, we detected chlorite in our XRD pattern. When comparing our results to the other mentioned clays, chlorite has two DHX temperatures biased on the OH environment. The first DHX temperature depends on the brucite layer and is at around 500 - 600 °C. The second stage represents the DHX signal of the talc layer, which appears at higher temperatures (47). This effect is easily observable in our XRD results (Figure 6). We also assume a thermal dissociation of carbonates for the hump at 790 °C. At around 980 °C and 1000 °C we see one more reaction that is not present in the reference material. This area can be interpreted as the DHX of biotite and the breakdown of the clay structures and the beginning of recrystallization. As mention in the XRD section, we could not find mullite but magnetite at higher temperatures.

5.5. SEM-EDS

Scanning electron microscopy with energy dispersive x-ray spectroscopy allows us to analyze our samples visually and in terms of the elemental composition of the samples respectively.

5.5.1. SEM

In Fig. 7 we show SEM images of various purified samples of Tiller Flotten clays. They reveal that the clay particles generally exhibit similar size distributions with edges that are not as sharply defined as the smooth flat faces. Moreover, we occasionally observe organic and calcite deposits.

Specifically, large organic particles with several tens to hundreds of μm in size were observed (Fig. 7 I). DTG and XRF results show that such organic matter accounts for less than 1% of the total sample mass in Tiller Flotten clays. However, it is known that even small amounts of OM can influence the soil's behavior significantly (48).

The calcite found in our samples was mainly due to the presence of fossilized foraminifera (Fig. 8 F). Based on Feyling-Hanssen (49), we assume that the shells of the micro-organism Elphidium incertum are present. We also found another type, which is only a few μm in diameter (Fig. 7 H). However, this fossil was not complete and therefore not indefinable.

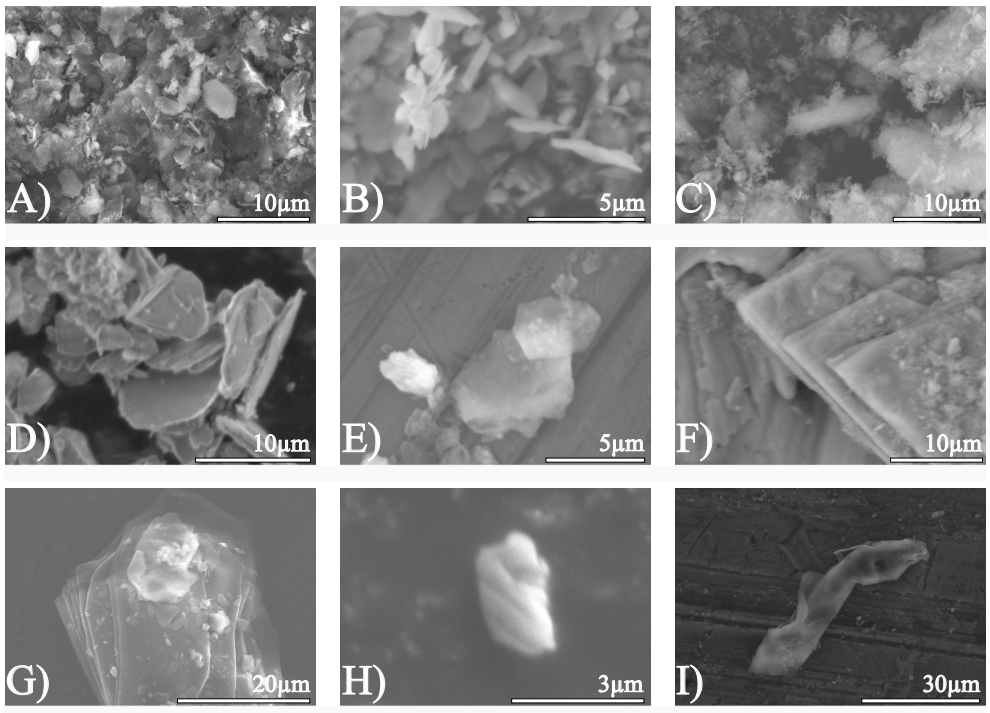

Figure 7: SEM pictures from our Tiller Flotten quick-clay samples from 7 m and 17 m. A) to C) Images taken from different probes of TF quick clay, showing different types of clays. Typical minerals also present are quartz and feldspar. Images in D) and E) show aggregates of clay minerals. F) Altered Biotite. G) Chlorite H) Foraminifer, not completely intact. I) Organic material.

5.5.2. EDS

EDS results provide an elemental analysis of the clay minerals in wt%, allowing us to calculate the oxides and thus the crystal structure of the clay mineral, using the formula proposed by Köster (50). Latter makes the general assumption that the total layer charge is neutral. Based on these computed crystal structures we were able to distinguish further between illite, muscovite, biotite and chlorite.

For our pure illite material we obtain the following crystal structure:

$$(K_{0.77})(Al_{2.12}Mg_{0.01})(Si_{2.85}Al_{1.15})O_{10}(OH)_2 \ .$$

Based on the mica nomenclature of the International Mineralogical Association (29), the illite series is defined by an amount of potassium ranging

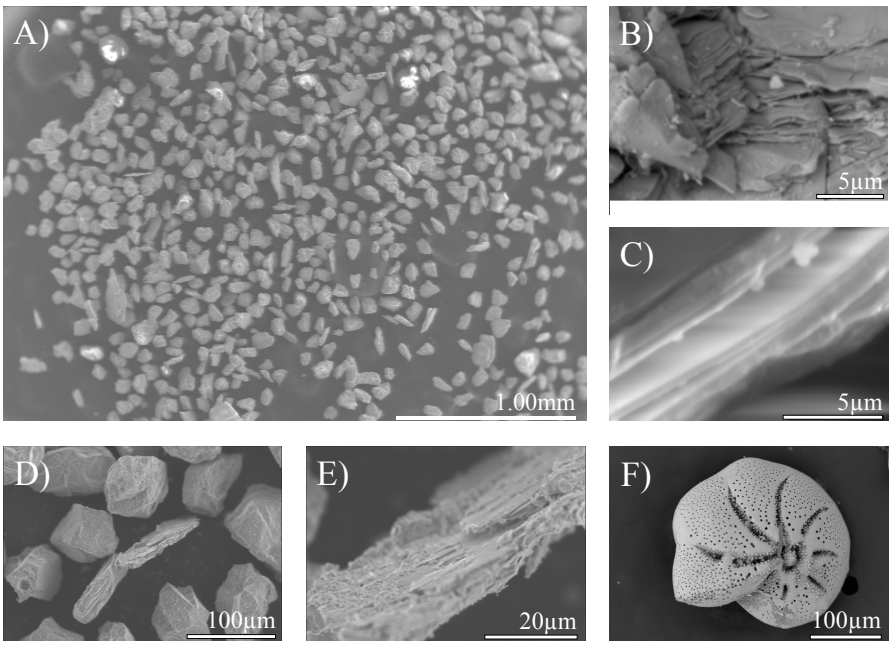

Figure 8: SEM images of the Tiller–Flotten quick clay fraction >63 μm. A) Overview of the sample, showing particles up to 0.3 mm in size. B) Clay aggregate with distinct layering of several clay minerals. C) Biotite particle. D) Aggregate composed of quartz, feldspar, and clay minerals. E) Higher-magnification image of the clay aggregate shown in D). F) Foraminifer (BSE image), tentatively identified as *Elphidium incertum*.

between 0.6 and 0.85 per half-cell. Our calculated value of 0.77 lies perfectly within that range.

We compared the crystal structures obtained from our EDS results with those we obtained from XRF measurements (see later) and the XRD data sheet of the pure illite from the supplier. Both XRF and XRD measures lead to very similar, calculated crystal structures. Since we know that TiO_2 (rutile, anatase, diaspore) is present in the sample, we removed Ti from the calculations.

Form the XRD values given by the supplier, we calculated a structure formula of

$$(K_{0.82}Na_{0.01}Ca_{0.01})(Al_{2.04}Mg_{0.02}Fe_{0.01})(Si_{2.96}Al_{1.04})O_{10}(OH)_2 \ ,$$

while the XRF measurement gives us

$$(K_{0.87}Na_{0.01})(Al_{2.02}Mg_{0.02}Fe_{0.01})(Si_{2.99}Al_{1.01})O_{10}(OH)_2 \ .$$

The calculated structures show an even higher K content, which is closer to the muscovite end member (29).

When comparing to the general formula for illite given by Grim:

$$(K \gg Na.Ca)_z(Al > Fe.Mg)_y(Si_{4-x}Al_x)O_{10}(OH)_2 \ ,$$

where $x = 0.43 - 0.66$, $y = 2.00 - 2.12$, and $z = 0.61 - 0.7$, we note that the pure illite sample contains not only a too high K content but also a higher substitution of Si by Al in the tetrahedral layer. This confirms our XRD observations that suggest that the commercially supplied illite contains a considerable fraction of muscovite.

For the Tiller Flotten quick clay we made over 200 measurements from samples taken at different depths and preparations. Our XRD measurements suggest the presence of illite, muscovite, biotite, and chlorite, which we also find back in our EDS results (see Fig.9).

Note that samples with high Mg and Fe content but little to no K we interpret as chlorite, while high K values with high Fe and Mg content indicate the presence of biotite.

We determined the average biotite structure:

$$(K_{0.96}Na_{0.15})(Al_{0.35}Mg_{1.07}Fe_{1.05})(Si_{2.48}Al_{1.42})O_{10}(OH)_2 \ ,$$

and the chlorite structure:

$$(K_{0.15}Na_{0.02}Ca_{0.02})(Al_{0.6}Mg_{0.57}Fe_{1.45})(Si_{2.49}Al_{1.51})O_{10}(OH)_2 \ .$$

The K value and the ratio between Mg/(Mg+Fe) and Al/(Al+Si) found in our samples fit the biotite structure perfectly (51).

Some measurements that were performed in different spots of the same samples show a K value at around 1 with an isomporphic (Si:Al) substitution of 3:1 in the tetrahedral sheet, containing little or no Fe or Mg. Their crystal structure is found to be

$$(K_{1.12})(Al_{1.93}Mg_{0.03})(Si_{3.23}Al_{0.97})O_{10}(OH)_2 \ ,$$

which represents a typical muscovite signature.

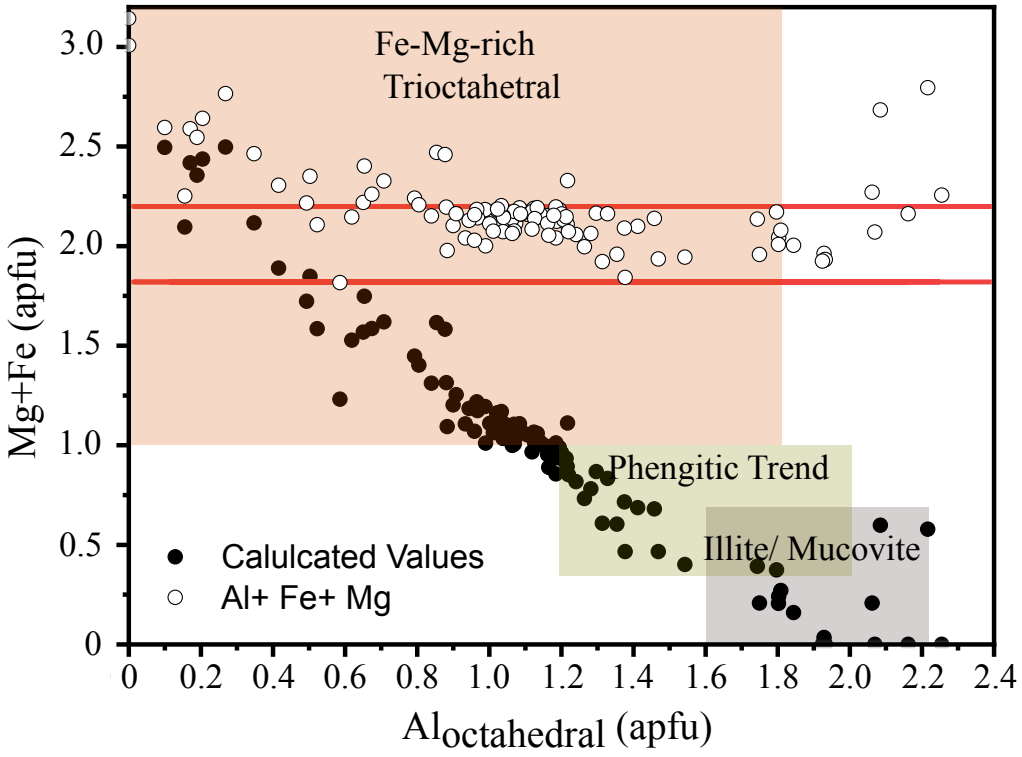

Figure 9: Calculated octahedral occupancies of the TF samples derived from EDS analyses. Black circles represent the Fe + Mg and Al contributions to the octahedral sheet, while open circles indicate the total octahedral occupancy. Red lines mark the occupancy range of 1.8–2.2 octahedral cations per half-unit cell. Total occupancies exceeding 2.2 are indicative of trioctahedral clay minerals.

For our illite we calculated an average crystal structure of

$$(K_{0.57}Na_{0.05}Ca_{0.03})(Al_{1.27}Mg_{0.31}Fe_{0.52})(Si_{3.26}Al_{0.74})O_{10}(OH)_2 \ .$$

This formula shows a slightly higher isomorphic substitution in the tetrahedral sheet than proposed by Grim. Nevertheless, the interlayer cation value and the Al/(Al+Fe) ratio align well with the nomenclature (29).

To ensure that our crystal structure calculations are correct we also tested the instrumental limitations and sample sizes. First, if the clay particles were thinner than about 5 μm and the electron beam had a high reaction volume, such that it passed through the sample an additional contribution from the underlying sample holder was measured. In this case an artificially high Al

Table 1: Clay mineral distribution based on EDS measurements

Tiller Flotten Quick Clay	Count	[%]
Illite	15	34,09
Muscovite	15	34,09
Biotite	1	2,27
Chlorite	13	29,55
Total	44	100,00

peak appeared. Secondly, in mixed samples, materials beneath the clay layer can contribute with a different elemental composition. For instance, the presence of feldspar or other clay minerals underneath or near the clay mineral of interest can influence the measured spectra. Despite these limitations, the large number of measurements conducted confirms that the structural formulas of the different minerals in our samples represent excellent estimates.

In Table 1 we list how often we found phyllosilicates in Tiller Flotten clay based on our EDS measurements.

The remaining specimens we measured have a similar base structure as illite but have less K in the interlayers and higher Fe and Mg content in the octahedral sheet. Those can be a) mixed signals of illite and chlorite, b) illite with smectic interlayers, c) Fe-Mg rich illite or d) altered biotite.

5.6. XRF

The XRF results in Table 2 provide quantitative amounts of the main oxides found in TF quick clay at different depths and in the pure illite sample. We note that the quantitative amounts of the single oxides in all TF quick-clay samples are similar and agree well with our EDS measurements. Moreover, they are in great agreement with previous XRF measurements made in the Tiller Flotten area (52).

Table 2 also shows that the amounts of F_2O_3 and Mg_2O decrease with depth, while the Na_2O_3 and CaO content increases gradually. We argue that the higher values are linked with the fresh water infiltration depth. In general, it should not be assumed that the chemical composition of the quick clay is homogeneous, since the clay amount deceases with depth (7). We should emphasize two additional points: (i) We only tested the composition in three different geological depths with random samplings. (ii) Although we measured similar amounts of oxides across all samples the actual mineral identity can vary from sample to sample.

Table 2: XRF measurements of Tiller Flotten quick clay for the depth 7m, 10m, and 17m as well as from the pure illite.

Oxides	XRF			
	QC 7m	QC 10m	QC 17m	Pure Illite
K_2O	4.21	4.47	3.98	10
Na_2O_3	1.89	1.9	2.05	0.04
CaO	3.11	3.30	3.45	0.06
SiO_2	50.6	49.4	51.5	43.9
Al_2O_3	17.5	17.7	17.2	37.7
MgO	6.38	6.27	6.06	0.16
TiO_2	0.783	0.767	0.779	1.63
Fe_2O_3	10	9.76	9.27	0.189
LOI 1000 °C	4.93	5.83	4.92	5.88
Total Oxides	94.47	93.57	94.30	93.68

In comparison, the pure illite sample contains more K_2O, Al_2O_3 and much more TiO_2, where later can be explained by the presence of rutile, anatase and diaspore. The much lower F_2O_3 and Mg_2O can the explained by the simple fact that the quick-clay samples also include other minerals as well as oxide minerals, which can be found in post-glacial sensitive marine clay deposits (53).

5.7. Specific Surface Area

5.7.1. BET

For the SSA we used the BET and methylene blue spot test. With the BET method we measured a SSA of 27.1 m^2g^{-1} for the TF17 and 12.36 m^2g^{-1} for the pure illite sample. We used laponite for additional control measurements. Laponite is a well studied synthetic clay that is based on the structure of hectorite. We determined it's surface area to be 344.36 m^2g^{-1}. The exfoliated laponite nano-discs are on average $23 - 30$ nm wide and 1 nm thick. Our result are in good agreement with previous studies (54).

5.7.2. Methylene Blue spot test

The other method is the methylene blue spot test. This is a highly common method for estimating the SSA of soils. We calculated the SSA following reference (55):

$$SSA = \frac{1}{MB_{MW}} \frac{m_{MB}}{m_{DI}} * (0.5N) * A_V * A_{MB} * \frac{1}{m_{soil}} \ .$$

Here, $\mathrm{MB_{MW}}$ is the molecular weight of methylene blue (319.87 $\mathrm{gmol^{-1}}$); $\mathrm{m_{MB}}$ is the dry mass of MB and m_{DI} the measured mass of added deionized water. N is the number of MB increments of 0.5 ml steps added to the soil solution; A_V is Avagadro's number ($6.02{\times}10^{23}\,\mathrm{mol^{-1}}$); A_{MB} is the area one MB molecule can cover, which is generally assumed to be $130{\times}10^{-20}\,\mathrm{m^2}$. For all experiments we used 1g MB for 200ml deionized water.

For sample TF7, 2 g of oven-dried material was used for the methylene blue test, resulting in a calculated SSA of $\sim 27.6\ m^2\mathrm{g^{-1}}$. For sample TF17, 10 g of oven-dried material was used, yielding an SSA of $\sim 28.2\ m^2\mathrm{g^{-1}}$.

These results are in good alignment with the BET results. Another work from (5) determined the SSA of quick clay in the Dragvoll area. They measured values of 18.3 - $27.8\,\mathrm{m^2g^{-1}}$. One should mention that the BET method usually provides slightly smaller SSA values than the MB method. This is due to the nitrogen molecules, which can only cover the external surface, while the methylene blue can also penetrate the space between non-exfoliated phyllosilicate sheets (56).

5.8. Cationic Exchange Capacity

Using the methyelne blue spot test allows us to estimate the CEC of the sample. The formula is given by

$$CEC = \frac{100}{W_S} * V_{MB} * N_{MB},$$

where W_{S} it the weight of the soil; V_{MB} is the added volume of MB and N_{MB} is the Normality of MB (55), which is given in equivalent per liter.

For our TF7 and TF17 samples we obtained CEC values of 3.5 eq/100g and 3.68 eq/100g, respectively. These values are significantly lower than those found in quick clays from the Dragvoll area(5), which were 6.3 - 7.7 eq/100g. Although it should be mentioned that the methyelene blue spot test we used usually provides a smaller CEC value than the NH4-Na method used in the Dragvoll study (5; 55).

5.9. Pore size

For TF17 we were able to perform both BET and BJH tests, which provided us with a respective pore size adsorption of 19.3 nm and desorption of 20.1 nm. These values lie within the range of meso-pore sizes (2-50 nm) reported in reference (57). Further, we obtained an average pore volume of 0.12 $cm^3\ g^{-1}$ for adsorption and 0.13 $cm^3\ g^{-1}$ for desorption measurements.

5.10. Particle size distribution

The particle size distribution has been measured with the classical hydrometer test and the Mastersizer 3000E. Both methods have been applied to the TF7 samples.

Assuming the general definition of clay, which only contain particle sizes that are smaller than $2\,\mu m$, roughly 62 % of our sample falls into that fraction, when using the hydrometer test. In comparison, only $\sim$ 19 % falls in this fraction in the Mastersizer test. Even if we adjust the clay particle size definition to $< 4\,\mu m$, we receive a potential contribution of $\approx$ 32 %. The comparison with earlier measurements of clay sizes for Tiller Flotten samples, which claim that $45 - 70$ % of the particle sizes obey the clay definition when using the hydrometer test, suggests that the Mastersizer test provides erroneous results (58)(7).

Furthermore, our hydrometer tests did not produce particle sizes $>73\mu$m, while the Mastersizer test finds that $\approx$ 10 % are in this fraction.

This large discrepancy fond in these two tests may be due to the differnt sample preparations required. Specifically, the Mastersizer required only short sonication times to rapidly attain stable results (within 5 min), while for the hydrometer test no sonnication was needed, however, the sedimentation times took up to 24 hours.

5.11. Zeta potential

Zeta potential measurements are important to understand the diffuse double layer of particles and therefore the interaction between particles. The strength of this Coulomb repulsion between the particles strongly influences the physico-chemical and mechanical properties of the ground (59). In 1981, Hunter stated "*it is impossible to overestimate the importance of electrokinetic effects, as they are fundamental to understanding an enormous variety of natural phenomena, such as the stability of colloidal suspensions*" (60).

For the pure illite we measured a zeta potential of -26.1 ± 1 mV at pH 8. Our TF7 and TF17 samples have a slightly higher value of -28.5 $\pm 2.3\,mV$ at a pH 8.03.

Today, researchers have started to install potassium wells for quick clay stabilization (3). Clearly, adding salt columns to the ground that gradually release cations has become a means to prevent sudden landslides in quick-clay rich ground. Therefore, we tested the effect of different salts on our quick clay, namely NaCl, KCl, MgCl, $CaCl_2$, KOH, and K_2CO_3 by measureing the particle's zeta potential (see Fig.10).

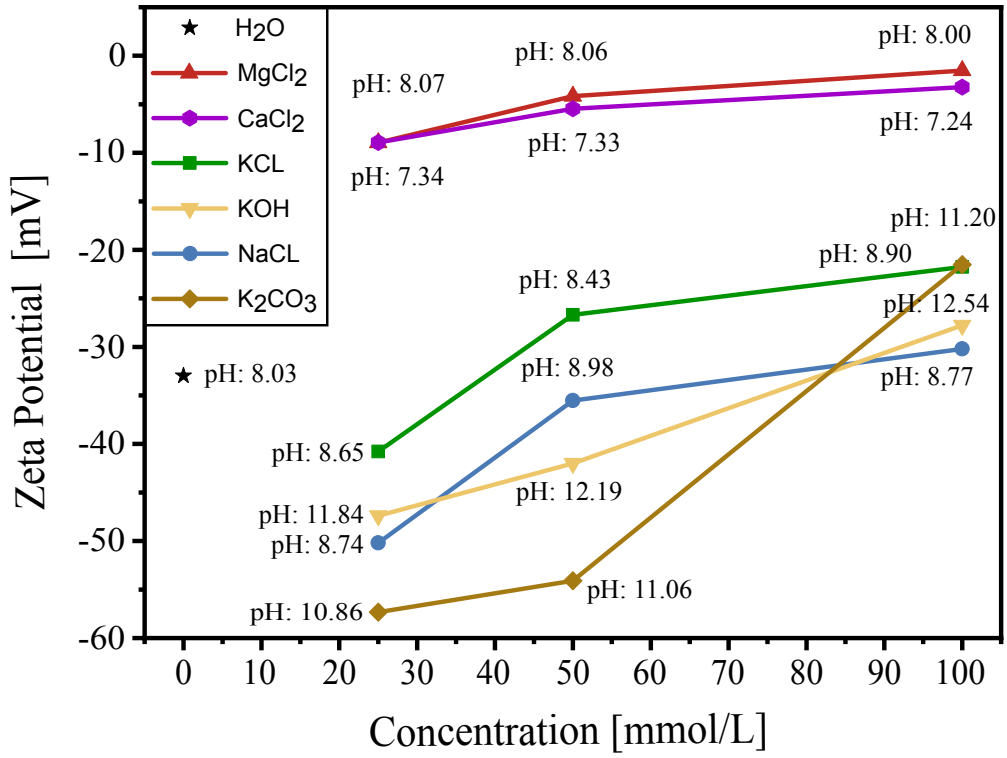

Figure 10: The effect of NaCl, KCl, MgCl, $CaCl_2$, KOH, and K_2CO_3 on the zeta potential of Tiller Flotten quick clay. Each salt has been tested with a concentration of 25, 50 and 100 [mmol L^{-1}].

The divalent cations in $MgCl_2$ and $CaCl_2$ lower the zeta potential significantly and reduce the stabilizing DDL almost completely, which leds to strong

flocculation and thus stabilization. On the other hand, low concentrations of added monovalent salts increases the DDL and only higher concentrations shorten the screening length, but not as efficiently as the divalent cations. This is a well-know effect (61). Although the stabilizing effect of $MgCl_2$ on soil is known (62), its effect on quick clay is less studied.

6. Discussion

The combined XRD, thermal analysis, BET, methylene blue and EDS results indicate that the mineralogy of the Tiller Flotten quick clay is much more complex than a simple illite-dominated assemblage. While illite was identified by XRD, the mineralogical data suggest that a significant proportion of the clay-sized phyllosilicates may consist of altered biotite rather than illite. The XRD analysis revealed a substantial biotite content, while thermal analysis showed a pronounced reaction between approximately 550 and 650 °C, which may be attributed to either illite or altered biotite. Furthermore, upon heating to higher temperatures, the TF7 sample formed magnetite, whereas the reference illite sample recrystallized to mullite. In addition, several EDS-derived structural formulas showed reduced interlayer potassium contents and compositions consistent with altered biotite.

The measured specific surface area of approximately $27\,m^2g^{-1}$ and the low cation exchange capacity of approximately 3-4 eq/100g are consistent with a mineral composition dominated by non-expanding clay minerals, including biotite, muscovite, illite, and chlorite. However, the occurrence of altered biotite and possible intermediate weathering products may explain the limited swelling behavior observed in the investigated samples.

Although the distinction between illite and altered biotite may have limited influence on the conventional geotechnical classification, it may be relevant for understanding the physicochemical processes governing quick-clay behavior. In particular, differences in surface charge, cation exchange capacity, and mineral reactivity may influence the interaction between clay particles and pore water, as well as the effectiveness of stabilization methods such as chemical additives and salt-well treatment. Further investigation of the clay-sized fraction is therefore recommended to better constrain the role of altered biotite in the behavior of Tiller Flotten quick clay.

7. Conclusion

In this study we investigated the mineralogical and physicochemical characteristics of Tiller Flotten quick-clay using X-ray diffraction (XRD), thermal analysis, scanning electron microscopy with energy-dispersive spectroscopy (SEM-EDS), BET surface area measurements, the methylene blue spot test and the clays zeta potential in the presence of different added salts. The results indicate that the mixture of minerals present is dominated by mica-group minerals, including biotite, muscovite, and illite, together with chlorite, quartz, and feldspars. While illite was identified by XRD, the combined XRD, thermal analysis, and EDS results suggest that altered biotite is the main clay mineral.

The investigated samples exhibited specific surface areas of $\sim 27\,\mathrm{m^2\,g^{-1}}$, in close agreement between the BET and methylene blue methods. The methylene blue derived cation exchange capacity was approximately $3-4$ eq per 100 g, indicating a relatively low surface charge density and supporting the predominance of non-expanding clay minerals. Despite the absence of significant amounts of expandable clay minerals, limited swelling was observed, which may be related to the presence of altered biotite and intermediate weathering products.

From a geotechnical perspective, the distinction between illite and altered biotite may not substantially affect conventional soil classification. However, it may be important for understanding the physicochemical mechanisms governing quick-clay behavior, particularly the interactions between mineral surfaces and pore-water chemistry. These interactions may influence both the sensitivity of the clay and its response to stabilization techniques. Further investigation of the clay-sized fraction is needed to better constrain the occurrence and role of altered biotite in Tiller Flotten quick clay.

Overall, the results presented in this study improve the understanding of the mineralogical and physicochemical characteristics of the Tiller Flotten quick clay. These findings provide important input parameters for future modeling and simulation studies (63) and may contribute to the development of more accurate conceptual and numerical models of quick clay behavior, both at Tiller Flotten and in similar quick clay deposits.

Acknowledgments

RT and EE are supported by the Research Council of Norway through its Centres of Excellence funding scheme (project no. 262644, PoreLab).

KDW as well as the PhD-studentships of RT and KZ are funded by the RCN Project 'Sustainable Stable Ground' (grant no. 324486).

Author Contributions

RT performed the sample preparation and the majority of the experimental data and structure analysis. KZ was involved in sample preparation and conduction of zeta potential and TGA measurements. RT and EE wrote the manuscript with inputs from all other authors.

Data Availability Statement

Data are available from the corresponding authors upon reasonable request.

Conflicts of interest

The authors have no conflicts of interest to disclose.

References

[1] P. Paniagua, J. L'Heureux, Comparison of three norwegian marine clays from a mineralogical, chemical and geotechnical approach, in: Proc. XVII European Conf. on Soil Mech. and Found. Eng., Reykjavik, Iceland, 2019.

[2] I. T. Rosenqvist, Norwegian research into the properties of quick clay—a review, Engineering Geology 1 (6) (1966) 445–450.

[3] T. E. Helle, M. Kvennås, B. Hamel, S.-A. Strand, G. Svanø, B. K. F. Bache, A. S. Gylland, E. Haugen, C. Sætre, T. Wiig, et al., Potassium chloride wells used as quick-clay landslide mitigation: installation procedures, cost–benefit analysis, and recommendations for design, Canadian Geotechnical Journal 59 (9) (2022) 1660–1678.

[4] W. Kirk, F. M. Synge, Farms of verdal, norway, Scottish Geographical Magazine 70 (3) (1954) 106–123.

[5] T. E. Helle, P. Aagaard, S. Nordal, M. Long, S. Bazin, A geochemical, mineralogical and geotechnical characterization of the low plastic, highly sensitive glaciomarine clay at dragvoll, norway, AIMS Geosciences 5 (4) (2019) 704–722.

[6] A. Emdal, M. Long, A. Bihs, et al., Characterisation of quick clay at dragvoll, trondheim, norway (2012).

[7] A. Gylland, M. Long, A. Emdal, R. Sandven, Characterisation and engineering properties of tiller clay, Engineering Geology 164 (2013) 86–100.

[8] M. Stork, W. Meindertsma, M. Overgaag, M. Neelis, A competitive and efficient lime industry: Cornerstone for a sustainable europe, European Lime Association: Brussels, Belgium (2014).

[9] S. Andavan, V. K. Pagadala, A study on soil stabilization by addition of fly ash and lime, Materials Today: Proceedings 22 (2020) 1125–1129.

[10] S. Ritter, P. Paniagua, G. Cornelissen, Biochar in quick clay stabilization: Reducing carbon footprint and improving shear strength, in: GeoCongress 2023, 2023, pp. 15–24.

[11] H. Nasiri, N. Khayat, M. Mirzababaei, Simple yet quick stabilization of clay using a waste by-product, Transportation Geotechnics 28 (2021) 100531.

[12] P. Bujulu, A. Sorta, G. Priol, A. Emdal, Potential of waste paper sludge ash to replace cement in deep stabilization of quick clay, in: Annual Conference of the Transportation Association of Canada Saskatoon, Saskatchewan, 2007, pp. 14–17.

[13] T. E. Helle, P. Aagaard, On the importance of mineralogy and geochemistry on the development of norwegian quick clays–a review and compiled datasets (2025).

[14] W. S. Broecker, G. H. Denton, R. L. Edwards, H. Cheng, R. B. Alley, A. E. Putnam, Putting the younger dryas cold event into context, Quaternary Science Reviews 29 (9-10) (2010) 1078–1081.

[15] A. Romundset, N. Akçar, O. Fredin, J. L. Andersen, F. Høgaas, M. Christl, S. Yesilyurt, C. Schlüchter, Early holocene thinning and final demise of the scandinavian ice sheet across the main drainage divide of southern norway, Quaternary Science Reviews 317 (2023) 108274.

[16] R. W. Berry, P. Jørgensen, Grain size, mineralogy and chemistry of a quick-clay sample from the ullensaker slide, norway, Engineering Geology 5 (1) (1971) 73–84.

[17] A. Kjemperud, Trondheimsfjorden, nord-trøndelag, norway.

[18] R. S. Liebling, P. F. Kerr, Observations on quick clay, Geological Society of America Bulletin 76 (8) (1965) 853–878.

[19] C. Chassagne, Introduction to colloid science: applications to sediment characterization, TU Delft OPEN Publishing, 2021.

[20] H. Van Olphen, An introduction to clay colloid chemistry, Soil Science 97 (4) (1964) 290.

[21] R. E. Grim, Modern concepts of clay materials, The Journal of Geology 50 (3) (1942) 225–275.

[22] S. Guggenheim, R. T. Martin, Definition of clay and clay mineral: joint report of the aipea nomenclature and cms nomenclature committees, Clays and clay minerals 43 (2) (1995) 255–256.

[23] F. Bergaya, G. Lagaly, K. Beneke, History of clay science: a young discipline, Developments in clay science 1 (2006) 1163–1181.

[24] A. Meunier, B. Velde, B. Velde, Illite: Origins, evolution and metamorphism, Springer Science & Business Media, 2004.

[25] R. E. Grim, R. H. Bray, W. F. Bradley, The mica in argillaceous sediments, American Mineralogist: Journal of Earth and Planetary Materials 22 (7) (1937) 813–829.

[26] T. Al-Ani, O. Sarapää, Clay and clay mineralogy, Physical-chemical properties and industrial uses (2008) 11–65.

[27] H. Gaudette, J. Eades, R. Grim, The nature of illite, in: Clays and Clay Minerals (National Conference on Clays and Clay Minerals), Vol. 13, Cambridge University ss & Assessment, 1964, pp. 33–48.

[28] S. J. Smith, Susceptibility of interlayer potassium in illites to exchange, Iowa State University, 1967.

[29] M. Rieder, G. Cavazzini, Y. S. D'yakonov, V. A. Frank-Kamenetskii, G. Gottardi, S. Guggenheim, P. W. Koval, G. Mueller, A. M. Neiva, E. W. Radoslovich, et al., Nomenclature of the micas, Clays and clay minerals 46 (5) (1998) 586–595.

[30] P. F. Kerr, Quick clay, Scientific American 209 (5) (1963) 132–143.

[31] C. B. Crawford, Quick clays of eastern canada, Engineering Geology 2 (4) (1968) 239–265.

[32] K. Carrado, A. Decarreau, S. Petit, F. Bergaya, G. Lagaly, Synthetic clay minerals and purification of natural clays, Developments in clay science 1 (2006) 115–139.

[33] X. Zhou, D. Liu, H. Bu, L. Deng, H. Liu, P. Yuan, P. Du, H. Song, Xrd-based quantitative analysis of clay minerals using reference intensity ratios, mineral intensity factors, rietveld, and full pattern summation methods: A critical review, Solid Earth Sciences 3 (1) (2018) 16–29.

[34] S. P. Bentley, N. J. Clark, I. J. Smalley, Mineralogy of a norwegian post-glacial clay and some geotechnical implications, The Canadian Mineralogist 18 (4) (1980) 535–547.

[35] S. Bentley, I. Smalley, Mineralogy of sensitive clays from quebec, The Canadian Mineralogist 16 (1) (1978) 103–112.

[36] Y. Kato, Mineralogical study of weathering products of granodiorite at shinshiro city (iii) weathering of primary minerals (2) mineralogical characteristics of weathered mineral grains, Soil Science and Plant Nutrition 11 (1) (1965) 30–40.

[37] S. Hov, P. Paniagua, C. Sætre, H. Rueslåtten, I. Størdal, M. Mengede, C. Mevik, Lime-cement stabilisation of trondheim clays and its impact on carbon dioxide emissions, Soils and Foundations 62 (3) (2022) 101162.

[38] A. Khaldoun, P. Moller, A. Fall, G. Wegdam, B. De Leeuw, Y. Méheust, J. Otto Fossum, D. Bonn, Quick clay and landslides of clayey soils, Physical review letters 103 (18) (2009) 188301.

[39] T. Helle, R. Bryntesen, H. Amundsen, A. Emdal, S. Nordal, P. Aagaard, Laboratory setup to evaluate the improvement of geotechnical properties from potassium chloride saturation of a quick clay from dragvoll, norway, Proceedings for GeoQuebec2015-Challenges from North to South, Quebec, Canada, 20–23 September 2015 (2015).

[40] R. S. Eilertsen, L. Hansen, T. H. Bargel, I.-L. Solberg, Clay slides in the målselv valley, northern norway: characteristics, occurrence, and triggering mechanisms, Geomorphology 93 (3-4) (2008) 548–562.

[41] W. Lieske, W. Baille, J. Schmatz, S. Kaufhold, R. Dohrmann, Characterisation of natural and remoulded onsøy clay with focus on the influence of mica, Engineering Geology 295 (2021) 106378.

[42] I. T. Rosenqvist, J. A. DONS, Marine clays and quick clay slides in south and central Norway, Norwegian Government's Organizing Committee, 1960.

[43] G. Wang, H. Wang, N. Zhang, In situ high temperature x-ray diffraction study of illite, Applied Clay Science 146 (2017) 254–263.

[44] G. Spray, M. Zaman, P. Hu, E. Harder, A widespread challenge: Differentiation of illite clay from muscovite mica for resource exploration and development.

[45] J. H. d. Araújo, N. F. d. Silva, W. Acchar, U. U. Gomes, Thermal decomposition of illite, Materials Research 7 (2004) 359–361.

[46] M. Földvári, Handbook of thermogravimetric system of minerals and its use in geological practice, Vol. 213, Geological Institute of Hungary Budapest, 2011.

[47] P. SCHNEIDER, P. TROPPER, W. WERTL, C. BERTOLDI, The breakdown behavior of chlorite at high temperatures: a combined high-t xrd and dta/tg study, in: 86th Annual Meeting of the German Mineralogical Society-DMG, Berlin, Germany, 2008.

[48] E. Ekwue, Organic-matter effects on soil strength properties, Soil and Tillage Research 16 (3) (1990) 289–297.

[49] R. Feyling-Hanssen, The stratigraphic position of the quick clay at bekkelaget, oslo, Norsk Geologisk Tidsskrift 33 (3) (1954) 185–196.

[50] H. M. Köster, Die berechnung kristallchemischer strukturformeln von 2: 1-schichtsilikaten unter berücksichtigung der gemessenen zwischenschichtladungen und kationenumtauschkapazitäten, sowie die darstellung der ladungsverteilung in der struktur mittels dreieckskoordinaten, Clay Minerals 12 (1) (1977) 45–54.

[51] X. Li, C. Zhang, H. Behrens, F. Holtz, Calculating biotite formula from electron microprobe analysis data using a machine learning method based on principal components regression, Lithos 356 (2020) 105371.

[52] S. Hov, K. Zabłocka, P. Paniagua, K. Weerdt, Elemental mapping by micro x-ray fluorescence to assess binder distribution of improved soils, Géotechnique Letters 14 (4) (2024) 158–162.

[53] J. K. Torrance, Oxide minerals in the sensitive post-glacial marine clays, Applied Clay Science 5 (4) (1990) 307–323.

[54] H. Pálková, J. Madejová, M. Zimowska, E. Bielańska, Z. Olejniczak, L. Lityńska-Dobrzyńska, E. M. Serwicka, Laponite-derived porous clay heterostructures: I. synthesis and physicochemical characterization, Microporous and Mesoporous Materials 127 (3) (2010) 228–236.

[55] Y. Yukselen, A. Kaya, Suitability of the methylene blue test for surface area, cation exchange capacity and swell potential determination of clayey soils, Engineering Geology 102 (1-2) (2008) 38–45.

[56] Y. Zheng, B. A. Baudet, Evolution of nano-pores in illite-dominant clay during consolidation, Acta Geotechnica 19 (1) (2024) 71–83.

[57] U. Kuila, M. Prasad, Surface area and pore-size distribution in clays and shales, in: SPE Annual Technical Conference and Exhibition?, SPE, 2011, pp. SPE–146869.

[58] J.-S. L'Heureux, A. Lindgård, A. Emdal, The tiller-flotten research site: Geotechnical characterization of a very sensitive clay deposit, AIMS Geosciences 5 (4) (2019) 831.

[59] M. Mojid, H. Cho, Estimating the fully developed diffuse double layer thickness from the bulk electrical conductivity in clay, Applied Clay Science 33 (3-4) (2006) 278–286.

[60] R. J. Hunter, Zeta potential in colloid science: principles and applications, Vol. 2, Academic Press, 2013.

[61] J. N. Israelachvili, Intermolecular and surface forces, Academic Press, 2011.

[62] N. Latifi, A. S. A. Rashid, S. Siddiqua, S. Horpibulsuk, Micro-structural analysis of strength development in low-and high swelling clays stabilized with magnesium chloride solution—a green soil stabilizer, Applied Clay Science 118 (2015) 195–206.

[63] G. Li, A. S. de Wijn, Molecular dynamics simulations of nanoscale friction on illite clay: Effects of solvent salt ions and electric double layer, Journal of Colloid and Interface Science (2025) 139107.